Growth of Branched Actin Networks against Obstacles

Anders E. Carlsson
Department of Physics, Washington University, St. Louis, Missouri 63130-4899 USA

ABSTRACT A method for simulating the growth of branched actin networks against obstacles has been developed. The method is based on simple stochastic events, including addition or removal of monomers at filament ends, capping of filament ends, nucleation of branches from existing filaments, and detachment of branches; the network structure for several different models of the branching process has also been studied. The models differ with regard to their inclusion of effects such as preferred branch orientations, filament uncapping at the obstacle, and preferential branching at filament ends. The actin ultrastructure near the membrane in lamellipodia is reasonably well produced if preferential branching in the direction of the obstacle or barbed-end uncapping effects are included. Uncapping effects cause the structures to have a few very long filaments that are similar to those seen in pathogen-induced "actin tails." The dependence of the growth velocity, branch spacing, and network density on the rate parameters for the various processes is quite different among the branching models. An analytic theory of the growth velocity and branch spacing of the network is described. Experiments are suggested that could distinguish among some of the branching models.

INTRODUCTION

The growth of actin networks is a crucial factor in the crawling mobility of almost all eukaryotic cells. The growth of such networks is believed to provide the force necessary for extending cell protrusions such as lamellipodia, and for propelling intracellular pathogens such as *Listeria* through the cytoplasm. Recent experiments (Loisel et al., 1999) have shown that motile forces can be generated by the actin polymerization energetics alone, without the help of motor proteins such as myosin. An important factor in understanding the nature of the network growth process is determination of the network structure. Numerous ultrastructural studies have been performed of the actin network in cells. Of particular interest here are studies of lamellipodia of fish keratocytes (Small et al., 1995; Svitkina et al., 1997), *Xenopus laevis* fibroblasts (Svitkina and Borisy, 1999), and *Xenopus laevis* keratocytes (Svitkina and Borisy, 1999), as well as the intracellular "comet tails" generated by *Listeria* (Small, 1988; Sechi et al., 1997). The lamellipodia studies provided a detailed picture, showing a dense branched structure with almost none of the branches oriented away from the membrane. Most branches were found to be at angles of $>30°$ relative to the growth direction. These structures have been described in terms of an idealized "orthogonal" network structure (Small et al., 1995; Svitkina et al., 1997) in which the branches grow at angles of 45° relative to the membrane, although the observed structures within 1 μm of the membrane are much more random than this idealized structure. Farther from the membrane, the orientations of the filaments are generally less random and correspond more closely the idealized model. We will reserve the term "orthogonal network" for this type of network structure, keeping in mind, however, that even here the observed networks are disordered. The attachment angle of the branches in the keratocytes was found to be quite constant (Svitkina et al., 1997), $75 \pm 10°$ relative to the growth direction of the filament. The *Listeria* studies revealed a structure based on two collections of filaments, one short and randomly oriented, and other long and oriented parallel to the motion. Very recently, studies have been performed (Cameron et al., 2001) of the comet tails induced in cell extracts by latex beads coated with the surface protein ActA. These studies have revealed a dendritic actin filament organization similar to that seen in the studies of lamellipodia.

Recent in vitro studies (Mullins et al., 1998; Welch et al., 1998) have demonstrated that branching can be stimulated by the Arp2/3 complex when activated by ActA, WASp (Wiskott-Aldrich Syndrome protein), or related proteins. The presence of the Arp2/3 complex in the environment of the polymerizing actin results in a branched network structure, and this complex is also found to be localized at the branch points of the network. The attachment angle, $70 \pm 7°$, is quite similar to that observed in fish keratocytes.

However, the type of branching found in these studies is not universal. Recent studies of *Rickettsia ricketsii* actin tails (Gouin et al., 1999; van Kirk et al., 2000), have shown a structure based mainly on long filaments (about a micron), with no evidence of a branched structure. Ultrastructural studies of carcinoma cells (Bailly et al., 1999) have revealed a network structure with a much greater variety of branching, including T-, Y-, and X-branching. The focus here is actin networks dominated by Arp2/3 complex-induced branching.

On the basis of ultrastructure studies such as those discussed above, along with detailed information about localization of cytoskeletal proteins, it is now generally accepted

Received for publication 20 February 2001 and in final form 11 June 2001.
Address reprint requests to Dr. Anders E. Carlsson, Dept. of Physics, Washington University, Campus Box 1105, One Brookings Dr., St. Louis MO 63130. Tel.: 314-935-5739; Fax: 314-935-6219; E-mail: aec@wuphys.wustl.edu.

0006-3495/01/10/1907/17 $2.00

that cellular networks in several types of cells result from branch formation caused by Arp2/3 complex activated by external signals, or proteins present on the surface of intracellular pathogens that "hijack" the actin polymerization machinery. However, the precise mechanisms of the network growth process are not understood. For example, it is not known whether branches are nucleated preferentially at the end (Pantaloni et al., 2000), or rather with uniform probability along the length of the filament (Blanchoin et al., 2000a). The orientational distribution of the branching is also not known. For example, there could be factors favoring branch nucleation in the growth direction of the network (Svitkina and Borisy, 1999). In addition, it is believed (Hartwig et al., 1995) that the cell membrane or the surface of an intracellular pathogen can have a barbed-end uncapping effect on the actin filaments, which would stimulate the network growth. This possibility has been supported by in vitro studies (Schafer et al., 1996), which showed that PIP_2 uncaps actin filaments. It has also been demonstrated that actin filaments induced by the Cdc42 protein are protected from capping (Zigmond et al., 1998; Huang et al., 1999). Finally, it is possible that cortactin stimulates actin network growth by inhibiting debranching (Weaver et al., 2001). The relative importance of these effects is not known.

If one understood the relationship between the branching and growth mechanisms on the one hand, and the structure and growth velocity of the network on the other hand, comparison with sufficiently detailed experiments could establish the nature of the important mechanisms. Several previous theoretical papers have addressed this relationship. A cellular automaton model (Dufort and Lumsden, 1993) has been used to study the spatial organization of actin gels. This model included a large number of biochemical mechanisms, including cross-linking and severing. However, it did not include the effects of Arp2/3-induced branching or an obstacle stimulating the growth; thus a meaningful comparison with cellular branched network structures was not possible. The Brownian-ratchet model (Peskin et al., 1993; Mogilner and Oster, 1996) has been used to derive the dependence of the growth rate on the orientation of a filament impinging on a membrane. It was found that an angle close to 45° is optimal. On this basis it was suggested that the orientation dependence of the growth rate could be responsible for the formation of the orthogonal actin networks referred to above.

The goal of the present paper is to provide a detailed analysis of the actin network growth rate, its three-dimensional structure, and the dependence of these properties on key rate parameters of the network growth process. This is accomplished by stochastic simulations of an actin network growing against an obstacle, keeping track of the positions of all the filament subunits over time. In this way the growth rate and all structural parameters of the growing network are accessible. The main approximations underlying the model are an approximate treatment of the network's flexural elasticity and its interaction with the obstacle, and neglect of electrostatic interactions, severing, cross-linking, and monomer-depletion effects. Some of the rate parameters are known, but for others values must be chosen to fit observed properties of the network.

From the simulation results I obtain three-dimensional visualizations of the growing network for eight distinct models involving different assumptions about the branching and growth mechanisms. These are compared with the ultrastructure studies of lamellipodia and *Listeria*-induced actin tails, and it is found that the structure near the membrane observed in lamellipodia is fairly well reproduced if a preference for branching in the direction of the obstacle, or barbed-end uncapping effects, are included. The inclusion of the uncapping effects results in a few very long filaments analogous to those seen in *Listeria* tails. However, I am unable to unambiguously pin down the correct model on the basis of these comparisons. I evaluate the dependence of the network growth rate, average spacing between branches along a filament, and network density near the obstacle on the simulation parameters, in particular the capping rate and the branching rate. I find pronounced differences among the models with regard to these dependencies. For the growth rate and the average branch spacing I present analytic theories. Finally, I propose experiments that can be performed to pin down which of the models are likely to be correct.

The organization of the remainder of the paper is as follows. The next section describes the model and its implementation. Subsequent sections give results for the three-dimensional network structure, dependences of the growth rate, average branch spacing, and network density on the simulation parameters, and an analytic theory for the growth rate and the average branch spacing. The last two sections give a critical discussion of the main approximations that are made in the calculations, conclude the paper, and suggest possible relevant experiments.

MODEL

The simulation procedure involves stochastic growth of a network from a starting configuration containing one or more seed filaments. The variables that are stored over time are the index numbers of the filaments, the positions of the subunits contained in each filament, the direction $\hat{n}$ of each filament, the capping state of the branched end of each filament, the collection of all the subunits in each filament that are branch points, and the index numbers of the filaments to which these subunits are attached. I do not track the capping state of the pointed ends of the filaments, but rather take all pointed ends to be uncapped. This will exaggerate the effects of pointed-end depolymerization. However, even with this exaggeration, I find that the effects of this process on the network structure and the growth rate are very small. Depolymerization would of course be an important factor in recycling monomers, but such recycling

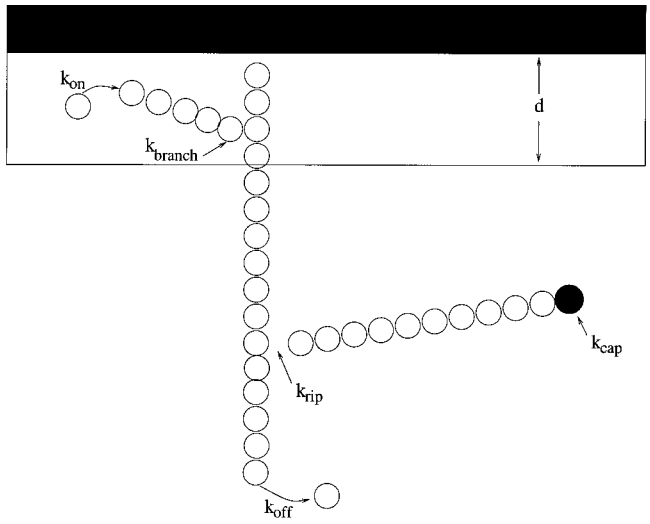

FIGURE 1 Schematic of unit processes in simulation method.

effects are not treated in the present work. Once a subunit is added to a filament, it does not move (although it can disappear). At each time step the following processes illustrated in Fig. 1 can occur, with probabilities determined by associated rate constants:

Growth

A monomer is added to the barbed end of an existing filament, at a distance $a = 2.7$ nm from the end. The position is determined by the filaments's direction vector $\hat{n}$. The filament is assumed to be straight and rigid, so $\hat{n}$ is a characteristic of the filament as a whole. This assumption is justified by the long persistence lengths that have been measured for actin filaments, ranging from 7 μm (Riveline et al., 1997) to 17–18 μm (Gittes et al., 1993; Ott et al., 1993; Isambert et al., 1995). The end of the filament in the direction of $\hat{n}$ is the barbed end, and the opposite end is the pointed end. The rate constant for monomer addition is k_{on}. All uncapped filament ends are potentially available for growth. However, steric exclusion effects reduce this number. These are taken into account by imposing a minimum distance of a between subunits. Thus, before adding each new subunit, it is necessary to scan all existing subunits to confirm that the site for the new subunit is sterically allowed. If done in the simplest fashion, this loop over all existing subunits would lead to a very slow code. To avoid this problem, I partition space into a three-dimensional cubic mesh and keep track of which subunits are stored in each mesh cube. Then, when adding a new subunit, it is necessary to scan only the subunits in mesh cubes adjacent to that containing the new subunit's position. This leads to a speedup factor of $\sim$100. I have increased the exclusion volume by a factor of $\sim$2.5, and see no substantial changes to the network structure, but only a 20% reduction in the network density.

Depolymerization

A monomer is removed from the pointed end, with rate constant k_{off}. This occurs only if the pointed end is not attached to another filament.

Capping

This simply involves a change in the integer variable for each filament that characterizes its capping state. The associated rate constant is k_{cap}. Once a filament has been capped, it remains capped forever and thus cannot grow. This assumption is justified by the small rate constants, $<10^{-3}$ s^{-1}, that have been measured (Schafer et al., 1996) for filament uncapping in the absence of potential uncapping agents at membranes.

Branching

A new "daughter" filament is attached to the side of an existing subunit (the "branching subunit"), with a rate constant k_{branch}. The variable describing the branching state of this subunit is changed accordingly. The daughter filament starts off with one subunit. It is possible that it has more than one subunit, but the starting number is not known. As long as this number is small in comparison with the branch spacing and the average filament length, its precise value will not be important. Depending on the model used (cf. below), new filaments can nucleate either with equal likelihood on any of the subunits in a filament, or only at the end of the filament. The position of the first subunit in the daughter filament is chosen at a distance of a from the branching subunit. The direction $\hat{m}$ from the branching subunit to the new subunit is chosen in the plane perpendicular to $\hat{n}$. The specific direction is chosen from all directions in this plane using a random number generator. The direction $\hat{n}'$ of the new filament is chosen to in the plane determined by $\hat{n}$ and $\hat{m}$, at an angle of 70° from $\hat{n}$, as suggested by the in vitro studies (Mullins et al., 1998) and cell studies (Svitkina et al., 1997). Electron micrographs have demonstrated the localization of Arp2/3 complex to branch points. I do not include this effect explicitly in my simulations. It could serve to shift the position of the first subunit in the new filament. However, we shall see later that the branch spacing and filament lengths substantially exceed the size of a single subunit, so this effect is likely to be unimportant.

Detachment of branches

The variable describing the branching state of a branched subunit is changed to the unbranched state, with a rate

constant k_{rip}. The pointed end of the filament that is detached is then available for depolymerization. The detached branch is not moved explicitly. However, it is assumed to diffuse away rapidly enough that it will not contribute to structures seen in electron microscopy studies.

The rate constants k_{on}, k_{off}, k_{cap}, k_{branch}, and k_{rip} are to be thought of as effective first-order rate constants in the sense that they include all concentration factors and thus correspond directly to the rates of the associated physical processes. The rates are implemented as follows. At each time step of length Δt, for each possible event (such as the addition of a monomer to a particular filament), a random number generator is used to generate a number x, such that $0 < x < 1$. If $x < k\Delta t$ (where k is any of the rate constants), the event occurs. The time step Δt is kept short enough that $k\Delta t \ll 1$ for all of the processes. Note that diffusion of the actin monomers and other proteins is not treated explicitly. By ignoring the time and spatial dependence of these concentrations, the model implicitly assumes that their diffusion is rapid in comparison with the processes of interest here, and that the reservoir of the proteins is large enough that depletion effects can be ignored. The validity of this assumption is discussed below.

The rate constants are determined by the concentrations of several proteins in the medium. Biochemical assays (Pollard, 1986; Pollard et al., 2000) have given the values $k_{on} = 11.6\ \mu M^{-1}\ s^{-1}\ c_a$ and $k_{off} = 1.4\ s^{-1}$, where c_a is the concentration of unpolymerized actin. The value of c_a varies widely from cell to cell; I use the value (Pollard et al., 2000) of 12 μM for *Xenopus* egg extract, which gives $k_{on} = 140\ s^{-1}$. For k_{cap}, values in the range 2.3–6.5 $\mu M^{-1}\ s^{-1}\ c_{cap}$ have been found in in vitro studies (Schafer et al., 1996), where c_{cap} is the capping-protein concentration. c_{cap} varies between cell types, and we are not aware of measurements for the *Xenopus* extract. However, in a broad range of cells one finds (Pollard et al., 2000) that the ratio c_a/c_{cap} of the free-actin to capping protein concentrations is between 40 and 100. This corresponds to a range of values of k_{on}/k_{cap} from ~100 to 300. In our simulations we typically use the value of 100, because this reduces the lengths of filaments emanating radially from the tail and thus permits easier visualization of the network structure near the obstacle. We find no significant differences in the small-scale network structure resulting from smaller values of k_{cap}. The major effect is a broadening of the tail, and of course an increase in the average filament length.

The rate constant k_{branch} should be determined by the concentration of activated Arp2/3 complex and the free actin concentration. However, the relationship between the Arp2/3 concentration and the branching rate is not known, particularly because Arp2/3 activation is an important factor. Therefore, it is not possible to determine this parameter a priori. Instead, k_{branch} is adjusted to correspond to observed branch spacings in electron micrographs (Svitkina and Borisy, 1999). Many branch spacings were found in a range centered roughly on 15 subunit sizes, and so I use this value here, except when I study the properties as a function of the branching rate. The growth velocity (scaled to the single-filament growth rate) and general nature of the structure depend mainly on the ratio of the branching rate to the capping rate, so the validity of the results is not unduly restricted by the choice of branch spacing. Branch detachment could occur spontaneously (Borisy and Svitkina, 1999), perhaps accelerated by ATP-ADP conversion, or be stimulated by proteins (Blanchoin et al., 2000b) such as actophorin and ADF/cofilin, or a combination of both. Again, the corresponding concentrations and rate constants are not known. I find that the structure of the network near the membrane is not affected by k_{rip}. However, the length of the tail is, and my strategy is to fix a value of the length of the tail and adjust k_{rip} so that the simulations match this value. The typical tail length is ~1 μm.

I note that the diffusion constant for actin monomers in cell cytoplasm is smaller than the in vitro values. In the cell cytoplasm, 3–6 $\mu m^2\ s^{-1}$ has been measured (McGrath et al., 1998), while the aqueous-solution value (Lanni and Ware, 1984) is 30 $\mu m^2\ s^{-1}$. The structure of the network near the obstacle will not be greatly influenced by such effects. Because an overall scaling of the rates will not affect the structure but only the time it takes for it to form, the structure will be determined by the ratios between the rates. For the structure near the obstacle, the important parameters are k_{on}, k_{cap}, and k_{branch}, and these are all determined by diffusion constants that are reduced in the cell environment. In addition, k_{rip}, which is the major factor in determining the large-scale structure of the actin tails, is likely to involve diffusion of proteins such as ADF/cofilin, and will thus be reduced in the cell environment as well. Therefore, my strategy is to use values of the rate constants corresponding to in vitro diffusion coefficients. The growth velocities that are obtained should then likely be scaled by a factor involving the diffusion constants.

I now turn to the interaction between the obstacle and the growing actin filaments. The obstacle is taken to be a 0.4-μm square. This value is used because it is the smallest size at which consistent growth is obtained for all of the models considered. In a few cases I have checked the results with obstacles up to about twice this size, and found the growth velocity and density to change only slightly. (In these cases I used mobility values reduced by a factor of the area increase, so that the force per unit area of the obstacle remained constant.) The lower face is at a position z_{obst}, and the obstacle moves only in the z-direction. The obstacle-filament interaction takes several forms:

1. Branching is allowed only in the vicinity of the obstacle. This assumption is based on the generally held view that the membrane against which the growing network exerts its force transiently activates the Arp2/3 complex. My implementation of this effect is to define a branching

region including the interior of the obstacle, and in addition a layer of thickness d extending down from z_{obst}. Branching is allowed to occur only within this layer. The correct value to use for d is not known. If branching occurs only when Arp2/3 attached to filaments is activated by physical contact with the membrane, then $d = 0$ would be appropriate. However, if activated Arp2/3 can diffuse from the membrane to the sides of growing filaments, then larger values are appropriate. In models defined below I distinguish between end branching and side branching. For the case of end branching the value of d has very little effect on the results, and I use $d = 0$. For the case of side branching I note that the density of branches along a portion of a filament inside the branching region should be proportional to $k_{branch}\bar{t}$, where $\bar{t}$ is the age of this portion of the filament. This means that parts of the network farther from the obstacle will have a larger branch density than those closer to the obstacle, and this growth will continue up to a distance of d from the obstacle. Such an increase is not observed in electron-microscopy experiments, which would resolve an increase in the branch density that took place over much more than a branch spacing. Therefore, I conclude that in the side-branching scenario, d does not exceed the branch spacing by a large factor. At small values of d, the end- and side-branching models are equivalent, because practically only filament ends can be inside d. Therefore, in my simulations for the side-branching scenario, I take d to equal the average branch spacing of 15 subunits;

2. The probability of subunits being added right at the obstacle is reduced because of a repulsive interaction with the obstacle. This locally reduces the rates for growth and branching by a factor of $\exp(-E/k_BT)$, where E is the interaction energy. Because capping involves a capping-protein molecule attaching at the end of a filament, I also apply such a factor to the capping rate. The interaction energy "turns on" when a prospective new subunit's z-coordinate z exceeds z_{obst}, and has the following form:

$$E = k_BT[(z - z_{obst})/\delta z]^3 \qquad (1)$$

where δz is the distance over which the energy becomes equal to k_BT. (Note that the choice of k_BT as the prefactor is purely a matter of convenience, because any change in the prefactor could be compensated by a change in δz.) The motivation for this form for the energy is that it has a steep climb after an initial smooth part. In a few cases I have tried other powers of the distance in the energy, ranging from 2 to 6. Over the range of values tried the velocity varies by ~2% and the density by ~25%. The general trends with the parameter values are unaffected. The smooth buildup of the energy is motivated by considerations of the elasticity of the networks. This elasticity means that if a filament is impinging on the obstacle, moving the obstacle down will not instantaneously result in an enormous energy jump for the system, as the filament can bend as a result of its own elasticity, the elasticity of branch points, or that of the rest of the network. For this reason, it is more appropriate to use a smoothed-out energy function than an abrupt one, and the quantity δz can be taken as a measure of the filament-end fluctuations present at room temperature. The most immediate source of filament-end fluctuations is the branch points. They have a thermal deviation (Blanchoin et al., 2000a) of 7° to 10°, which corresponds to a deviation of the filament end position of 1.5–2 subunit sizes if one takes the part of the filament beyond the last branch point to have a length of 15 subunits, the average branch spacing. For this reason, I use $\delta z = 2a$ in the simulations. Because there are many other sources of network elasticity, including filament bending, it is likely that the true value is larger than this. In my simulations with larger values of δz the density increases, but the other properties of the network remain basically unchanged. For very small values of δz, less than a, the network often fails to grow consistently at all. For each force exerted on a filament end, an equal and opposite force, in the z-direction, is exerted on the obstacle;

3. The obstacle follows a diffusional law of motion, so that for each time step

$$\Delta z = r(t)\sqrt{6D_{obst}\Delta t} + F_{obst}D_{obst}\Delta t/k_BT, \qquad (2)$$

where $r(t)$ is a random number between -1 and 1, D_{obst} is the diffusion coefficient of the obstacle (related to the mobility by the k_BT factor), and F_{obst} is the sum of all the individual filament forces acting on it. If I use values of D_{obst} calculated from the obstacle size and standard estimates of the viscosity of cytoplasm, the obstacle rapidly diffuses away from the filaments so that they no longer branch and the network stops growing. This is in line with the observation (Olbris and Herzfeld, 2000) that the filaments must be attached to the obstacle in some way to prevent it from diffusing away. Recent laser-tracking experiments (Kuo and McGrath, 2000) on *Listeria monocytogenes* have also found that the position fluctuations of the bacterium are so small as to require an attachment mechanism for their explanation. For this reason I choose values of D_{obst} to provide reasonable values of the polymerized-actin density for networks having the average branch spacing of 15 subunits. We choose 1 mM as the polymerized-actin density (Pollard et al., 2000). I note that an obstacle moving according to an equation of motion of the form of Eq. 2, together with the Boltzmann factor in the monomer-addition probability, naturally obeys an exponential force-velocity relation of the form proposed by Oster and collaborators (Peskin et al., 1993; Mogilner and Oster, 1996). The validity of this form has been confirmed by recent Brownian dynamics simulations (Carlsson, 2000).

TABLE 1 Summary of models considered

	Orientation Restriction of Branching	End Restriction of Branching	Uncapping
A1	No	No	No
A2	Yes	No	No
B1	No	Yes	No
B2	Yes	Yes	No
C1	No	No	Yes
C2	Yes	No	Yes
D1	No	Yes	Yes
D2	Yes	Yes	Yes

Although there is substantial consensus in the literature regarding the importance of Arp2/3-induced network branching at the growth front, the details of this process are not well established, and I thus consider several versions of the model that differ in their incorporation of additional effects that have been proposed in the literature. These models are summarized in Table 1.

- Model A1. This is the model outlined above, with branching allowed uniformly along the side of filaments. The possibility of such side branching is demonstrated by optical microscopy studies (Blanchoin et al., 2000a) of filaments grown in vitro;
- Model A2. This is the same as model A1, except that only branches pointing toward the obstacle are allowed. Potential branches pointing away from the obstacle are reflected through the filament so that they point toward it. This is motivated by the suggestion (Svitkina and Borisy, 1999) that a factor favoring branching toward the obstacle may be present, based on the predominance of such branching in observed ultrastructures. It is also consistent with the generally accepted activation mechanism (Higgs and Pollard, 2000) of Arp2/3, which follows the path (PIP2 or Cdc42) $\rightarrow$ WASp $\rightarrow$ Arp2/3, or one similar to it. Because PIP2 and Cdc42 are probably localized to the membrane, this would favor branch nucleation on the upper sides of filaments impinging the membrane;
- Model B1. This is the same as Model A1, except that branching is allowed only at filament ends. This model is supported by kinetic studies (Pantaloni et al., 2000) of polymerization kinetics and by comparison of mother-daughter branch lengths (Pantaloni et al., 2000; Cameron et al., 2001);
- Model B2. This differs from model B1 in that only branching toward the obstacle is allowed;
- Model C1. This model is like A1, except that it includes uncapping effects at the obstacle, motivated by the discussion in the Introduction. We include them in the limit that the uncapping is infinitely rapid in a layer of thickness d_{uncap} next to the obstacle, so that capping is effectively absent in this layer. This may also be thought of in terms of capping suppression in the vicinity of the obstacle. To avoid having too many independently changing variables, I do not scan a range of values of d_{uncap}, but rather use the value $d_{\mathrm{uncap}} = 3a$ except for a small number of test calculations. For smaller values the effects on the observed structure are small, but the capping-rate dependence of the growth rate and other parameters is still strongly affected. For larger values the structures begin to be dominated by very long uncapped filaments;
- Model C2. This model is the same as C1 except that only branching toward the obstacle is allowed;
- Model D1. This model is the same as C1 except that only end branching is allowed;
- Model D2. This model is the same as D1 except that only branching toward the obstacle is allowed.

THREE-DIMENSIONAL NETWORK STRUCTURE

I begin with a visual examination of the small-scale aspects of the structures that are formed in the eight models defined above. These are shown in Fig. 2. Here the light gray region denotes the obstacle and is displaced in the growth direction by four subunit spacings to avoid obscuring the subunits that enter the obstacle region. The main geometrical parameter that can be seen in these pictures is the distribution of orientations of the filaments. In this figure and Fig. 3 each subunit is indicated by a cone with its apex toward the pointed end of the filament. The size of the cones is chosen to be several monomer sizes in order to correspond more closely to electron micrographs. I delete filaments that are disconnected from the main body of the network, on the assumption that they diffuse away.

Visual examination of the structures suggests that the inclusion of side versus tip branching causes only small differences between the structures. In other words, the models divide into pairs (A1, B1), (A2, B2), (C1, D1), and (C2, D2), where the members of a pair give very similar structures. This is confirmed by quantitative analysis of the filament orientations. Following an earlier convention (Svitkina et al., 1997), I divide the filaments into "up" filaments, with angles of $<70°$ from the growth direction, "sideways" filaments with angles between 70° and 110° from the growth direction, and "down" filaments with angles of $>110°$ from the growth direction. I weight the filaments according to how much of their length is contained in a box of the dimensions of the obstacle, extending 40 monomer spacings into the network. The distributions of filament orientations are shown in Table 2. I consider the models in each pair together because the fractions in each pair are within two percentage points of each other.

From Table 2 one sees that the most important factor in distinguishing between the models is whether downward branching is allowed. Forbidding downward branching increases the up-fraction by $\sim$20%. The inclusion of uncapping also has a substantial effect in models that allow

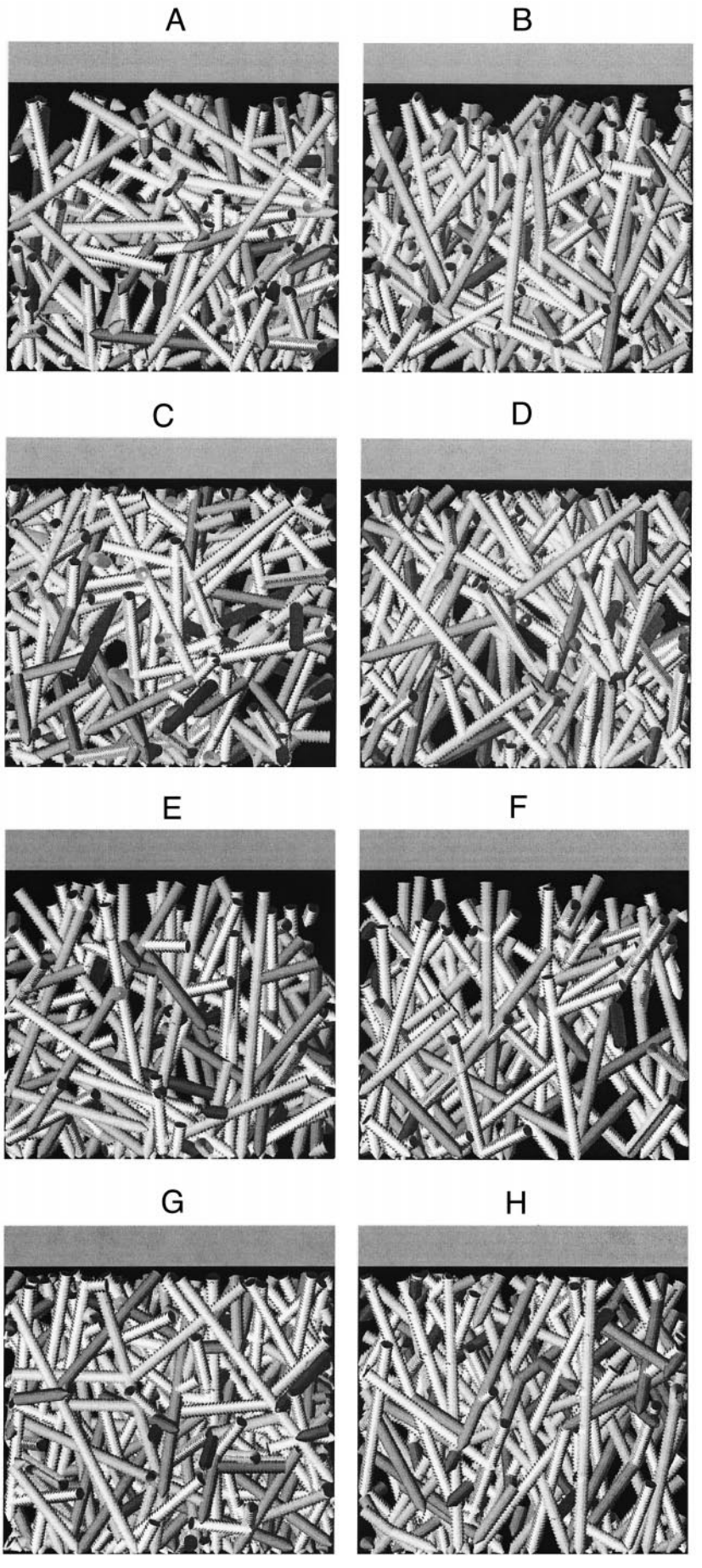

FIGURE 2 Near-obstacle structure of actin network for eight models defined in text. (*a*) Model A1; (*b*) model A2; (*c*) model B1; (*d*) model B2; (*e*) model C1; (*f*) model C2; (*g*) model D1; (*h*) model D2.

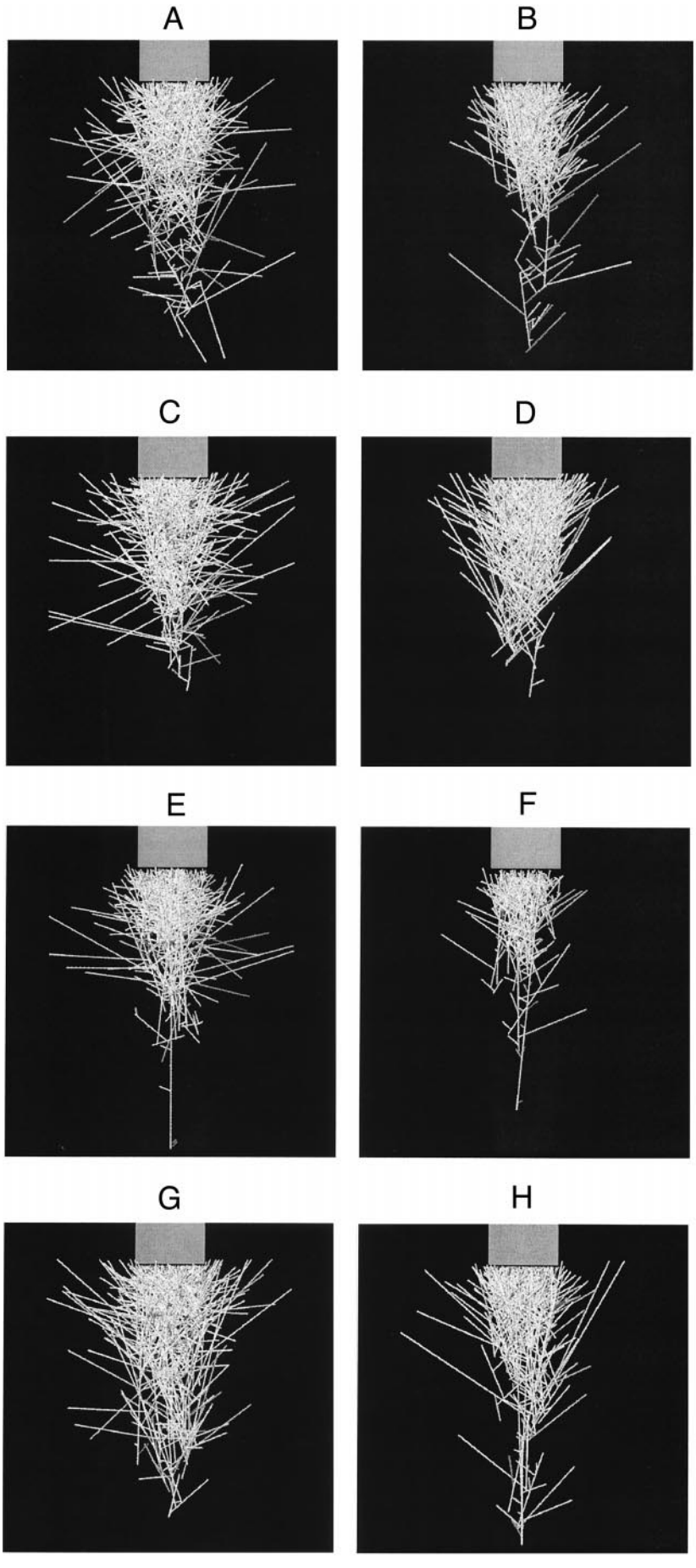

FIGURE 3 Large-scale structure of actin network for eight models defined in text. (*a*) Model A1; (*b*) model A2; (*c*) model B1; (*d*) model B2; (*e*) model C1; (*f*) model C2; (*g*) model D1; (*h*) model D2.

TABLE 2 Percentages of filaments having up, side, and down orientations, as defined in text

	Up	Side	Down
A1, B1	69	27	4
A2, B2	94	5	0
C1, D1	77	22	1
C2, D2	96	4	0

downward branching, thus the structures divide into three subsets: (A1, B1), (C1, D1), and (A2, B2, C2, D2). Visually, the (A1, B1) structures may be characterized as being the most random; however, they still have many more up than down filaments. The (A2, B2, C2, D2) structures are the most ordered and give the most sense of a directionally grown structure. They are, in fact, reminiscent of the "orthogonal networks" found in some ultrastructure studies (Small et al., 1995; Svitkina et al., 1997). I note, however, that the present simulations do not directly correspond to the orthogonal networks because these are found at distances of >1 μm from the membrane. The (C1, D1) structures are intermediate between the most and least ordered classes. In these structures very few down filaments are seen, even though they are in principle allowed. The uncapping effects in these models lead to a few very long filaments near the growth direction, and many of the branches come from these long filaments. These branches cannot be in the down category because of the 70° branching angle.

In visual examination, the structures coming from models (C1, D1) and (A2, B2, C2, D2) compare favorably with the electron microscopy studies of Svitkina and collaborators (Svitkina et al., 1997; Svitkina and Borisy, 1999), while models (A1, B1) are too disordered. In Svitkina et al., (1997) the fractions of up, sideways, and down filaments were found to be 75% up, 20% sideways, and 5% down. This would be closest to the values from models C1 and D1. Another possibility would be that downward branches are not entirely forbidden, but only disfavored. In other words, one could interpolate between models A1 and A2 or B1 and B2. Assuming downward branching to be suppressed by 30% would lead to values of 77% up, 20% side, and 3% down, close to the measured values. I note that the electron microscopy extraction procedures, along with disorder in the branching angles and that resulting from bending of filaments, will tend to enhance the disorder in the system, reducing the number of filaments in the "up" category. These effects will bring models A1 and B1 farther from the observed values and models A2 and B2 closer to them. This will increase the amount of downward branching suppression needed to match the data. However, I am not able to choose one model on the basis of the orientation distributions. The most likely alternatives are a member of the set (C1, D1), or a variation of (A2, B2) or (C2, D2), which allows some downward branching.

I turn now to the large-scale structure of the simulated actin networks, shown in Fig. 3. Models A1, A2, B1, and B2 yield largely similar structures. Away from the obstacle, the width of the tail gradually decreases. In A1 and B1 a long sparse extension of the tail is seen; however, this extension is seen in some runs and not in others, depending on the choice of seed for the random number generator. It is sometimes seen in models A2 and B2. Models C1, C2, D2, and several other runs of D1, show a different behavior far from the obstacle. They have a few very long filaments whose orientation is fairly close to the growth direction. These long filaments are found in most of the runs, but not always. The survival of a few long filaments far from the obstacle is not surprising for these models: the suppression of barbed-end capping allows the growth of very long filaments, and shorter filaments at this distance from the obstacle will detach at long times. Small and collaborators (Small, 1988; Sechi et al., 1997) have emphasized the presence of such long filaments in comet tails from intracellular pathogens. In addition, the studies on fish keratocyte lamellipodia (Svitkina et al., 1997) showed that the network more than roughly a micron from the leading edge was dominated by filaments several microns or more in length. The presence of these long filaments gives strong reason to take these models based on barbed-end capping suppression seriously.

QUANTITATIVE MEASURES OF STRUCTURAL AND GROWTH PROPERTIES

In this section I present numerical results for the parameter dependences of the growth velocity, the average branch spacing, and the density of polymerized actin at the obstacle. For the dependence of the growth velocity and the average branch spacing on k_{branch} and k_{cap}, I also present simple analytic theories. In evaluating quantitative measures of growth and structure a considerable amount of statistical averaging is necessary to obtain precise values. The variation in density between runs with different starting seeds for the random number generator is typically $\sim$15% or less at densities above 0.5 mM. To reduce this variance, I average over 20 runs for each set of values of the rate parameters. This reduces the statistical fluctuation by a factor of $1/\sqrt{20}$, to $\sim$3%. The fluctuations in the growth velocity and branch spacing are $\sim$1% and 2%, respectively. At lower densities the fluctuations in the network density increase, to $\sim$7% at 0.2 mM.

Growth velocity

Fig. 4 shows the dependence of the growth velocity on k_{cap} and k_{branch} for the eight models defined above. In this plot and the subsequent ones, I scale the values of k_{cap} and k_{branch} by k_{on}, so that k_{cap} can be thought of roughly as the inverse

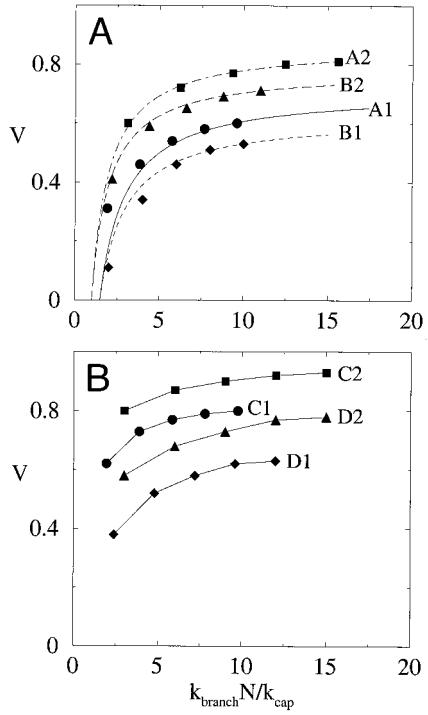

FIGURE 4 Dependence of obstacle velocity on k_{branch} at $k_{cap} = 0.01\ k_{on}$. V given in units of k_{on}. (*a*) Models A1 (*circles*), A2 (*squares*), B1 (*diamonds*), and B2 (*triangles*). (*b*) Models C1 (*circles*), C2 (*squares*), D1 (*diamonds*), and D2 (*triangles*). Curves in (*a*) are from analytic theory described in text.

of the average filament length. The growth velocity is scaled to that of a free uncapped filament, which is k_{on}. In the plots of the k_{branch}-dependence of the growth velocity we use the quantity $k_{branch}N/k_{cap}$ as the abscissa. Here N is the number of subunits available for branching in a straight filament impacting the obstacle, which is 1 for the end-branching models and taken to be $(d + \delta z)/a \cos 45° = 24$ for the side-branching models, where the cos 45° factor assumes an average orientation of 45° of the filaments relative to the growth direction. This choice is made because $k_{branch}N/k_{cap}$ then corresponds roughly to the number of branches per filament. The curves for models A1, A2, B1, and B2, shown in Fig. 4 *a*, all have a similar behavior. They approach an asymptotic velocity substantially below the free-filament velocity at large k_{branch} and drop off for small k_{branch}, with the dropoff accelerating around $k_{branch}N/k_{cap} = 4$. As expected, models A2 and B2, which enforce branching in the direction of the obstacle, have higher growth velocities than the corresponding unrestricted-branching models by ~25%. At first glance it is somewhat surprising that the end-branching models B1 and B2 have lower growth velocities then the corresponding side-branching models A1 and A2. To explain this effect, I have looked in more detail at the distribution of filament orientations. We define a "vertical filament" as one whose orientation is within 20° of the growth direction. Evaluating the fractions of vertical filaments as before, I then find that in models A1 and A2 10–11% of the filaments are vertical, while in models B1 and B2 only 6–7% are. There are thus ~50% more vertical filaments in models A1 and A2. With the relatively small forces exerted on the filament tips in the present simulations, the filaments pointing in the direction of growth have the highest growth rate (projected on the growth direction). Thus models A1 and A2 should have higher growth rates than models B1 and B2. Similar arguments apply to models C1 and C2, which contain ~14% vertical filaments and D1 and D2, which contain 5% vertical filaments. The larger absolute difference between the numbers of vertical filaments is reflected in a larger difference of model C1 relative to D1, and C2 relative to D2, which is seen in Fig. 4 *b*. The reason for the greater prevalence of vertical filaments is that the nucleation of a vertical filament requires a previous mother filament fairly close to horizontal. Such a filament will quickly drop back from the growth front. In the tip-branching model, in which physical contact with the membrane is required for nucleation, this filament will then be less likely to nucleate a daughter filament than it would be in the case of side branching.

Other aspects of the results for models C1, C2, D1, and D2 are quite parallel to the models without barbed-end capping suppression. The main difference is that the k_{branch}-dependence is somewhat weaker. This is to be expected because the velocity of an uncapped filament growing over a long distance against the obstacle will not be directly sensitive to branches growing off it. There will, however, be an indirect sensitivity because the branching rate will affect the number of filaments sharing the opposing force of the obstacle.

Fig. 5 *a* shows results for the k_{cap}-dependence of the growth velocity for the models without capping suppression. In all cases a monotonic dropoff is seen. The behavior is very linear. The largest fractional effects are seen for models A1 and B1, with model B1 experiencing a 60% velocity dropoff as k_{cap} goes from $0.005\ k_{on}$ to $0.025\ k_{on}$. In the parallel results for models C1, C2, D1, and D2 the k_{cap}-dependence is much weaker, which is to be expected if the filaments that remain uncapped over large distances are playing an important role.

The measured dependences (Loisel et al., 1999) of the velocities of pathogens on the protein concentrations are quite different from the rate dependences found here. The measured velocities show an optimal concentration for each protein rather than the monotonically increasing or decreasing values seen in Figs. 4 and 5. I believe that the observed behavior is due to "funneling" effects (Carlier and Pantaloni, 1997), in the sense that having a sufficiently small Arp2/3 concentration or a sufficiently large capping-protein concentration concentrates free monomers in the vicinity of the membrane. These effects are not present in our model because we assume a fixed monomer concentration.

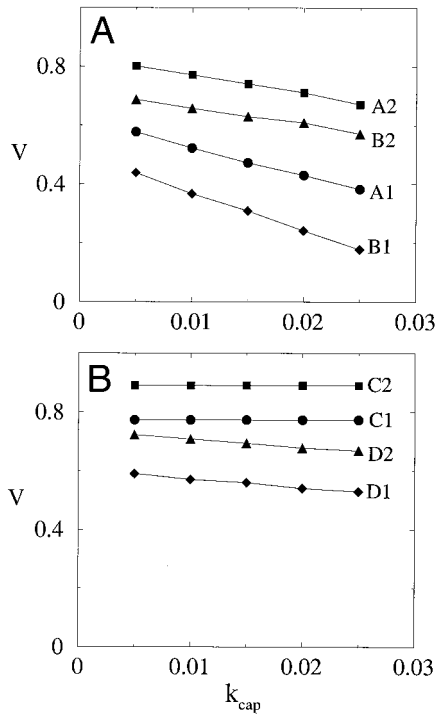

FIGURE 5 Dependence of obstacle velocity on k_{cap}, with branch spacing of 15 subunits at $k_{cap} = 0.01\ k_{on}$. k_{cap} and V given in units of k_{on}. (*a*) Models A1 (*circles*), A2 (*squares*), B1 (*diamonds*), and B2 (*triangles*). (*b*) Models C1 (*circles*), C2 (*squares*), D1 (*diamonds*), and D2 (*triangles*).

The numerical results can be clarified by developing a simple analytic model theory. Because the filament length, determined by the barbed-end capping rate, greatly exceeds the branch spacing, I focus on the case $k_{cap} \ll k_{branch}$. The case of models B1 and B2 is the simplest. In these models the branching occurs essentially at the same time that the branching subunit is added; otherwise this subunit would no longer be at the end. Thus, the time to cover a given growth path (defined by a given set of branchings) is simply proportional to the number of subunits in the path. The basic physics of the growth velocity is then that a high branching rate increases the velocity by allowing a higher fraction of the filaments at the growth front to have optimal orientations. Denote the average number of branches per filament by M. I note that even though there is no constraint on the branching directions in model B1, there will be very few branches pointing straight down; these would have to nucleated off down-pointing filaments, and these will rapidly move out of the branching region. In practice, there are very few filaments pointing $>120°$ away from the growth direction, and I use this as an upper limit in the theory. Because the branch orientations are spread over the surface of a sphere, their direction cosines are assumed to be spaced uniformly over the interval cos 0° to cos 120° for model B1. One readily shows that on the average, the direction of the best of the M branches of a filament is $\cos 0° + (1/M)(\cos 120° - \cos 0°) = 1 - 1.5/M$. A similar analysis applies to model B2, with 120° replaced by 90°. The resulting growth velocities are then

$$V = k_{on}[1 - 1.5k_{cap}/k_{branch}] \quad \text{B1} \tag{3}$$

$$V = k_{on}[1 - 1.0k_{cap}/k_{branch}] \quad \text{B2}. \tag{4}$$

These results are plotted in Fig. 4 *a*, with an adjustment of the overall magnitude of the velocity to match the last calculated point in each curve. It is seen that the fit to the numerical data is quite good, in particular the difference between models B1 and B2 with regard to the reduction in k_{branch} required to cause a 50% reduction in velocity. Similarly, Fig. 5 *a* confirms the linear k_{cap} behavior predicted by the simple theory. The slopes are also fairly commensurate with those of the theory. The theory predicts reductions of 60% and 30%, respectively, at $k_{cap} = 0.025\ k_{on}$ relative to $k_{cap} = 0.005\ k_{on}$ for models B1 and B2; the simulation values are 60% and 20%.

For models A1 and A2 I use a parallel analysis, simply replacing k_{branch} by Nk_{branch}. Then the growth velocities become

$$V = k_{on}[1 - 1.5k_{cap}/Nk_{branch}] \quad \text{A1} \tag{5}$$

$$V = k_{on}[1 - 1.0k_{cap}/Nk_{branch}] \quad \text{A2}. \tag{6}$$

The plots of these results in Fig. 4 *a* show similar accuracy to the results for the end-branching models, except for model A1. Here, the value of k_{branch} at the 50% point is overestimated by about a factor of 3/2. The reductions at $k_{cap} = 0.025k_{on}$ for A1 and A2 are predicted to be 55% and 20%, respectively, in comparison with the numerical results of 35% and 15%.

I do not have a satisfactory theory for the growth in the models involving barbed-end capping suppression. The curves in Fig. 4 *b* could be fitted by a combination of the functions used in Fig. 4 *a* and a constant, but I see no merit in providing such a fit with out knowing what the relative weight of the constant term should be.

Branch spacing

Figs. 6 and 7 give corresponding results for the average branch spacing. This is evaluated inside a 40-subunit-thick box from the obstacle. All of the curves in Figs. 6 *a* and *b* decay monotonically with k_{branch}. This is expected since the branch spacing should be inversely proportional to k_{branch}. The curves in Fig. 7 *a* also reveal a monotonic decrease in average spacing as a function of k_{cap}. The curves in Fig. 7 *b*, for models with barbed-end capping suppression, show a weaker dependence on k_{cap}.

To develop an analytic theory for these effects I consider a filament having the average filament length, $l = k_{on}/k_{cap}$, and evaluate the average distance to the first branch. This is equivalent to evaluating the average distance between

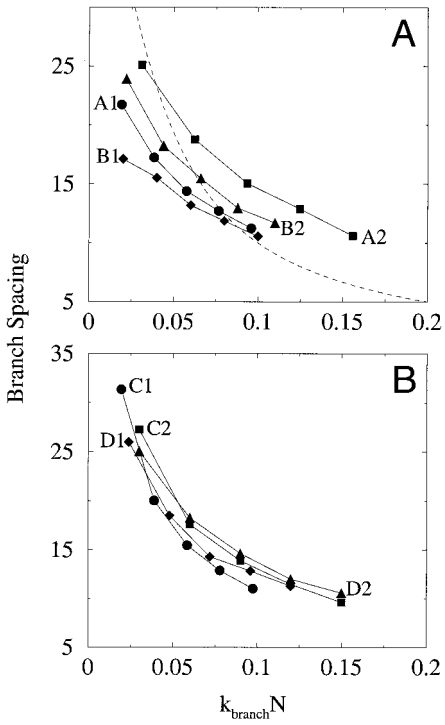

FIGURE 6 Dependence of average branch spacing on k_{branch}, at $k_{cap} = 0.01\ k_{on}$. k_{branch} is given in units of k_{on}. (*a*) Models A1 (*circles*), A2 (*squares*), B1 (*diamonds*), and B2 (*triangles*). (*b*) Models C1 (*circles*), C2 (*squares*), D1 (*diamonds*), and D2 (*triangles*). The dashed curve in (*a*) is analytic theory described in text.

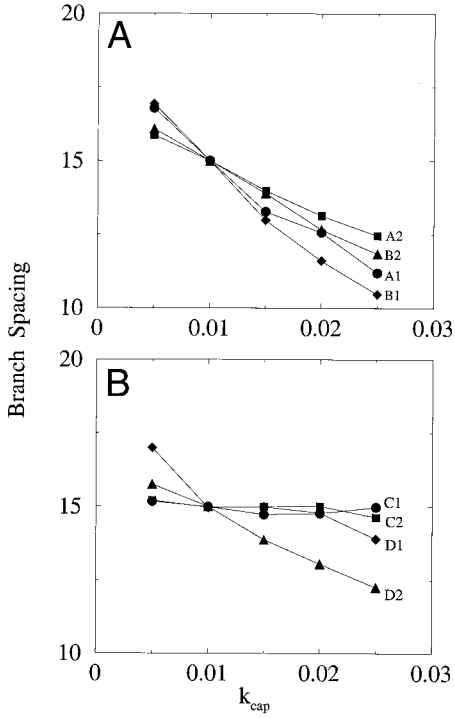

FIGURE 7 Dependence of average branch spacing on k_{cap}, with branch spacing of 15 subunits at $k_{cap} = 0.01\ k_{on}$. k_{cap} is given in units of k_{on}. (*a*) Models A1 (*circles*), A2 (*squares*), B1 (*diamonds*), and B2 (*triangles*). (*b*) Models C1 (*circles*), C2 (*squares*), D1 (*diamonds*), and D2 (*triangles*).

branches because the average length of a filament beyond any branch point is also *l*. This holds because the monomer-addition events are assumed to be uncorrelated. For simplicity, I first choose units in which $k_{on} = 1$, and begin with the case of end-branching. Then one readily shows that the probability of having no branches before subunit *m* along the filament is proportional to $\exp(-mk_{branch})$, so the probability of having the first branch at subunit *m* is proportional to $k_{branch}\exp(-mk_{branch})$. The average distance to the first branch is thus

$$\bar{m} = \frac{\sum_{m'=0}^{l} m' \exp(-m'k_{branch})}{\sum_{m'=0}^{l} \exp(-m'k_{branch})}. \quad (7)$$

By converting to an integral, which is appropriate because $k_{branch} \ll k_{on}$ and $k_{cap} \ll k_{on}$, we obtain

$$\bar{m} = \frac{k_{on}}{k_{branch}}\left[1 - \frac{n_{branch}}{\exp(n_{branch}) - 1}\right], \quad (8)$$

where $n_{branch} = k_{branch}/k_{cap}$ is the average number of branches per filament and we have gone to a general value of k_{on}. This result reduces to $\bar{m} = k_{on}/k_{branch}[1 - n_{branch}\exp(-n_{branch})]$ for $n_{branch} \gg 1$, the limit of interest here. This result is plotted in Fig. 6 *a*. It is seen that the prediction has roughly the correct magnitude and rate of dropoff with increasing k_{branch}. However, the rate of increase at small k_{branch} is lower in the numerical data. I believe that this is partly due to the finite size of the obstacle, which prevents an infinite branch spacing even as k_{branch} goes to 0. For the k_{branch} parameters used in Fig. 7 *a* the theory predicts 30% and 20% reductions at $k_{cap} = 0.025\ k_{on}$ for models B1 and B2, respectively. The corresponding reductions from the simulation data are 35% and 25%.

For the side-branching models I follow the same theory, replacing k_{branch} by Nk_{branch} as above. This yields capping-induced reductions of 25% for model A1 and 10% for model A2. This ordering is consistent with the corrections seen in Fig. 7 *a*, but the predicted correction for model A2 is substantially smaller than that obtained in the simulations.

Network density

Figs. 8 and 9 show the dependence of the density on k_{branch} and k_{cap}. It is averaged over the same box as the branch spacing. In all cases the density increases with k_{branch}, as expected. The increase is roughly linear. Fig. 9 *a* and *b* show that increasing k_{cap} reduces the network density, which is also expected because of the reduced average filament length. The effect seen in Fig. 9 *b* is smaller, as expected. Comparison of Figs. 8 and 4 indicates that over a range of values of k_{branch} the network density increases, but the velocity is essentially unchanged. This is consistent with

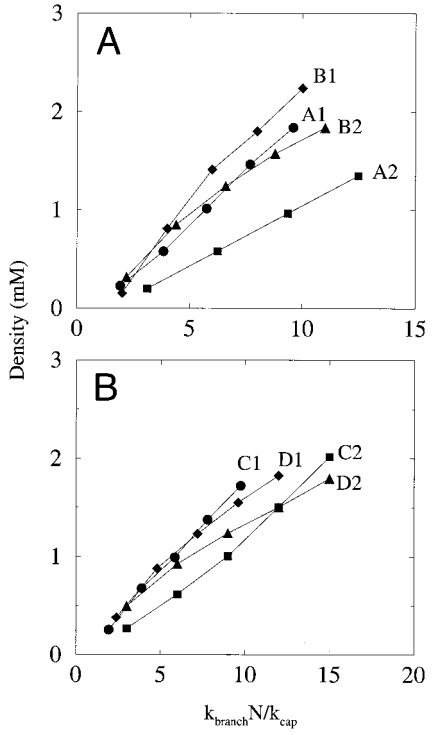

FIGURE 8 Dependence of network density on k_{branch}, at $k_{cap} = 0.01\ k_{on}$. (*a*) Models A1 (*circles*), A2 (*squares*), B1 (*diamonds*), and B2 (*triangles*). (*b*) Models C1 (*circles*), C2 (*squares*), D1 (*diamonds*), and D2 (*triangles*).

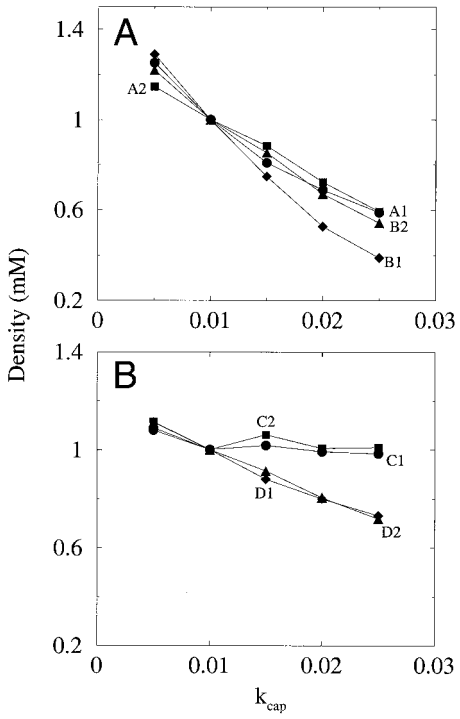

FIGURE 9 Dependence of density on k_{cap}, with density of 1 mM at $k_{cap} = 0.01\ k_{on}$. k_{cap} is given in units of k_{on}. (*a*) Models A1 (*circles*), A2 (*squares*), B1 (*diamonds*), and B2 (*triangles*). (*b*) Models C1 (*circles*), C2 (*squares*), D1 (*diamonds*), and D2 (*triangles*).

studies of latex beads (Cameron et al., 1999), which found that changing the bead coverage by ActA had a pronounced effect on the density but little effect on the velocity.

Developing a theory of the steady-state polymerized-actin density at the obstacle is difficult because the existence of a steady-state density is inherently a nonlinear effect due to the interactions between filaments, either direct or mediated by the obstacle. To see this, note that the simplest linear theory of the time evolution of the density in the case of end branching, in the frame of reference of the moving obstacle, would have the form

$$\frac{\partial \rho}{\partial t} = k_{branch}\rho + V_{obst}\frac{\partial \rho}{\partial z}, \qquad (9)$$

where ρ is the density of filament ends and the second term on the right-hand side is a convective derivative. This equation models the autocatalytic growth behavior of ρ. For a linear equation such as this, or a more complex linear equation, the solution at large times is a linear function of the initial conditions. Thus there can be no well-defined steady-state density at large times, independent of the initial conditions. In the simulations I find that there is such a density, which does not depend on how many filaments are used to seed the system. Therefore, nonlinear terms in ρ are necessary, which correspond to interactions between filaments.

Two possibilities for these nonlinear interaction terms come to mind. The first is the steric exclusion effects. I feel that these are not the dominant effect here. As mentioned above, expanding the exclusion volume around a subunit by up to a factor of 2.5 changes the steady-state density by only 20%. Furthermore, by using obstacles with extremely low mobilities, I have achieved network densities nearly 10 times higher than the highest ones obtained in the low-force limit. Therefore, steric exclusion effects are still fairly small in the cases treated here. Another possibility for the nonlinear interaction terms determining the actin density is an effective interaction mediated by the obstacle. As one filament grows, it pushes the obstacle forward so that it has less likelihood of nucleating new branches on other filaments. The higher the density of filaments, the faster will be the leading filaments, and the larger the probability that an average filament will leave the branching region before branching. Effectively, the average branching rate is reduced by a high density of filaments. The sensitivity of the density to the obstacle mobility, which I find below, is consistent with a filament-filament interaction mediated by the obstacle.

Effect of varying force

Fig. 10 *a* shows the effect of the obstacle force on the growth velocity. The force is varied by changing the mo-

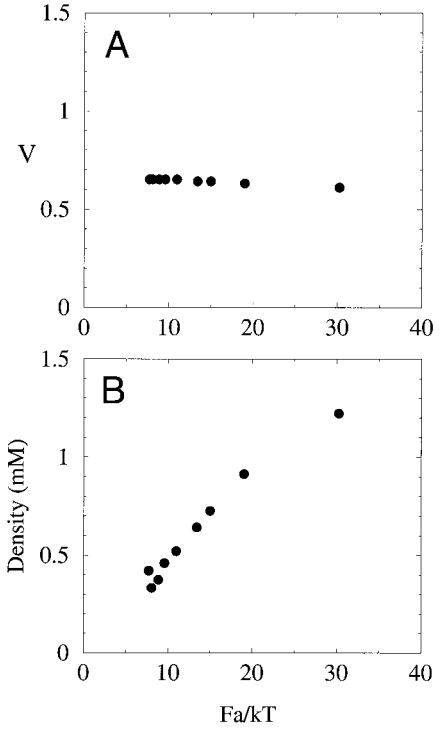

FIGURE 10 Effects of obstacle force on growth properties for model B2 with $k_{cap} = 0.01\ k_{on}$. (*a*) Growth velocity; (*b*) network density.

bility of the obstacle. It is seen that the effect on the growth rate is quite small, which is surprising given that single filaments obey an exponential decay law. As the force increases, the force per filament in fact remains rather constant as the number of filaments in contact with the obstacle increases. In other words, a self-regulating effect is controlling the velocity. This is illustrated in Fig. 10 *b*, which shows the force dependence of the network density. The density is quite linear as a function of the force. I believe that this effect is due to the fact that as the force increases, the leading filaments will push into the obstacle (or bend, actually), allowing other filaments to remain in contact with the obstacle and thus to keep branching and growing.

CRITIQUE OF MODEL

There are several approximations made in the model that prevent it from providing a complete description of the phenomena described. In this section I go through the major approximations and assess the impact that they are likely to have on the calculations.

Neglect of electrostatic interactions between filaments

Actin is well known to carry a substantial charge per subunit, exceeding 10 electron charges (Tang and Janmey, 1996) if cation condensation effects are not included. The effects of these charges are reduced both by the condensation effects and by Debye-Huckel type screening. It is not known how strong these effects are. However, under favorable circumstances it is possible for actin to self-assemble into structures (Wong et al., 2000) in which the interfilament spacing is as small as 7.5 nm, or about 3*a*. Eventually, the electrostatic interactions will serve to limit the network density and to cut off the type of increase with applied force seen in Fig. 10 *b*. It is not known at what densities this effect becomes dominant.

Neglect of monomer depletion effects

These can arise from depletion in the medium as a whole, or from diffusion-rate effects. As discussed above, depletion of the medium could lead to pronounced effects on the dependence of the network properties on the rate constants. For the purpose of comparing to in vitro experiments, there are enough biochemical data available that for a given experiment one should be able to evaluate the free-monomer concentration in the medium. However, establishing the dependence of parameters such as k_{branch} on this concentration will require assays that have not been performed yet. In any case, it should be possible to arrange experiments in which the monomer concentration is constant.

To assess the magnitude of the diffusion-rate effects I perform an approximate diffusion calculation. As mentioned above, the value of the diffusion coefficient of actin monomers in the cell cytoplasm has been measured (McGrath et al., 1998) to be 3–6 $\mu m^2\ s^{-1}$ and the aqueous solution value to be 30 $\mu m^2\ s^{-1}$ (Lanni and Ware, 1984). To make the estimate we consider actin network growth against a 0.4-μm square obstacle, as in the simulations. I take a typical value of the number of growing filament ends, 1370 μm^{-2}, from recent standing-wave fluorescence microscopy measurements (Abraham et al., 1999), which gives 220 filaments pushing against the obstacle. To evaluate the extent to which the free-actin concentration is depressed by the growth of the network, I model the area of growth as a spherical region of radius 0.2 μm. The concentration far away from this region is fixed at the cellular value c_a. Using rate and concentration parameters discussed above, the monomer current flowing into the polymerization region is $140\ s^{-1} \times 220 = 30{,}000\ s^{-1}$. Application of standard diffusion theory, using the aqueous-solution value of the diffusion constant, shows that this leads to a depression $\delta c_a = 0.4\ \mu M$ of the concentration at the edge of the polymerization region. Use of the cytoplasmic diffusion constant would give the same value, because the monomer current would be reduced by the same factor as the diffusion constant. Since δc_a is small in comparison with c_a, the approximation of neglecting the diffusion-rate effects is probably accurate for an obstacle of the size that we are considering. However, as the obstacle grows in size, the

monomer current grows proportional to the square of the obstacle size, which makes δc_a proportional to the obstacle size. Therefore, for an obstacle several microns in size, the diffusion-rate effects would become important.

Similar considerations apply to the concentrations of capping protein and Arp2/3 complex. The rate of consumption of capping protein is equal to that of actin monomers divided by the average filament length. If one takes the above value of 100 subunits for the average filament length and a value of 70 for the actin/capping protein concentration ratio, and assumes that the diffusion constant of capping protein is the same as that of actin, one finds that the fractional change in capping protein concentration at the edge of the polymerization region is ~70% of that in the actin concentration. The typical ratio of the concentrations of free actin and Arp2/3 complex (Pollard et al., 2000) is 20 to 30. Assuming a branch spacing of 15 subunits, this leads to a fractional reduction in the Arp2/3 concentration of about twice that for free actin monomers.

Neglect of severing effects

These should affect mainly the large-scale structure of the networks. They would reduce the probability of having very long filaments, such as those seen in Fig. 3 *b*.

Neglect of cross-linking effects

The extent of cross-linking varies a great deal among cell types, and the present model applies only to those where the cross-linking effects are small. Velocity measurements of pathogens in pure protein solutions (Loisel et al., 1999) found only small effects from cross-linking proteins.

Neglect of explicit terms accounting for filament elasticity and elasticity of branch points

As mentioned above, filament and branch point elasticity are accounted for, to some extent implicitly, by the δz term in the energy (Eq. 1). However, long-ranged relaxations of the actin tail are not included. Even though a one-micron tail is shorter than the persistence length of actin filaments, a single filament of this length would easily bend when acted on by relatively weak forces, but on the scale of the close-up "snapshots" (Fig. 2), the filaments should be essentially straight. Although the variations $\delta\theta$ in branching angle reported in previous studies (Svitkina et al., 1997; Mullins et al., 1998) are only 10° and 7°, respectively, the freedom for a filament to bend by an amount $\delta\theta$ of this magnitude could result in significant effects on the growth. For example, if the growth of a 20-subunit-long filament of is blocked by another filament, changing the filament orientation by 7° would move its end by two subunit sizes, which could easily be enough to avoid the blockage.

Neglect of orientational preferences in branching

Actin filaments do not have circular symmetry, as assumed here. The two dimers residing roughly side-by-side at any point along the filament define an orientation that rotates along the filament with a periodicity of 36 nm or 13 subunit spacings. If one assumes that the Arp2/3 complex adopts a particular orientation with respect to the dimers, then branches with a spacing corresponding to this filament periodicity should point in the same direction, rather than having a random orientation. One would expect this to enhance the degree of order in the network, but the precise nature of this ordering is not clear.

Neglect of ATP-ADP conversion

In general, monomers are incorporated into the growing filament in an ATP-bound state, but gradually convert to the ADP-bound state. The binding affinity for Arp2/3 to the filament and the rate of branch detachment are expected to be dependent on this conversion. Because all the branches forming in the model are formed near filament barbed ends, ATP-ADP conversion is likely not relevant for branch formation. In addition, the rate constant k_{rip} for branch detachment may be thought of as incorporating the effects of this conversion. On the whole, I believe that the lack of explicit treatment of ATP-ADP conversion in the model does not have serious consequences.

Neglect of attachment of filaments to the obstacle

As mentioned above, an attachment mechanism must be present to maintain contact between the filaments and the obstacle. I have not included this effect because the details are too poorly understood. The most illuminating studies of the effects of filament attachment are provided by recent laser-tracking studies (Kuo and McGrath, 2000) of *Listeria monocytogenes* moving through COS7 cells. These studies revealed a stepwise motion of periodicity 5.4 nm (twice the step size used in our simulations). It was also found that the fluctuations of the obstacle (the bacterium) are extremely small, on the order of 0.1 nm. The present model does not reproduce this behavior. Instead, the motion of the obstacle is mainly a smooth linear function with a random component superimposed; this random component is considerably larger than 0.1 nm. Inclusion of an attachment mechanism in the present simulations would definitely reduce the random component of the obstacle motion, conceivably to the level found in the laser-tracking data. Whether it would reproduce the 5.4 nm step size is unclear. Potential growth mechanisms that would lead to the discrete step size include those in which a single filament either leads the growth or limits it. Discrete steps would also occur if the motion occurs by concerted growth of several filaments aligned

with each other. I am not aware of evidence supporting either of these mechanisms. Another effect of attachment, if it prevented lateral motion, would be bending of the filaments and orientation of the filaments parallel to the direction of motion.

CONCLUSIONS

The main results of the above simulations are of two types. With regard to the three-dimensional structures, the favorable comparison of the simulated structures from several of our models with the lamellipodium ultrastructure studies suggests the presence of a bias for branch formation in the growth direction, or barbed-end uncapping effects, or both. The similarity of the structures obtained with uncapping effects to ultrastructure studies of *Listeria* tails, and to some extent those of lamellipodia, suggests that such uncapping effects are present in some cases. Studies of tails induced by other types of bacteria (Gouin et al., 1999; van Kirk et al., 2000) have shown structures almost entirely dominated by long parallel filaments. Thus it is possible that the range of structures shown in such tails means that in some cases uncapping effects are dominant, in others important, and in others negligible.

With regard to the quantitative measures of network properties, I have made specific predictions about the dependences of the growth rate, branch spacing, and density on the key rate parameters. For comparison with the present results, it would be desirable to make measurements of these quantities at fixed concentration of free actin monomers. If this concentration changes, the rate parameters will vary in a fashion that is not known. The most directly testable of the predictions is the dependence of the growth velocity on the capping rate at fixed branching rate, shown in Fig. 5 *a* and *b*. The rate k_{cap} here is proportional to the capping-protein concentration. One could measure this dependence by using asymmetrically ActA-coated beads in a protein mixture, in experiments analogous to those performed on motion of beads in a cell extract (Cameron et al., 1999). In this case, one identifies the growth velocity of the network with the relative velocities of the bead and the treadmilling tail. To set up an experiment corresponding to the simulations, one would start with a concentration of activated Arp2/3, and then adjust the capping protein concentration so that $k_{on}/k_{cap} = 13l_{branch}$, where l_{branch} is the average branch spacing. (This corresponds to scaling the $k_{cap} = 0.005k_{on}$ points in Fig. 5, *a* and *b* to the value of l_{branch} in the experiments, which may not have the value 15 subunits used as the baseline in this paper.) Then one would increase the capping-protein concentration by a factor of 5. Under these circumstances, the models predict rather different decreases of the growth rate: 35% for A1, 15–20% for A2 and B2, 60% for B1, 0% for C1 and C2, and 10% for D1 and D2. These differences are large enough to make meaningful experimental distinctions.

Another useful class of experiments that would serve to test the whole approach used here involves velocity measurements at a fixed k_{branch}/k_{cap} ratio. All of the models predict weak dependences of the velocity on the magnitude of k_{branch} and k_{cap} if this ratio is fixed. For example, starting at a k_{branch} value corresponding to $l_{branch} = 15$ subunits, and $k_{cap} = 0.015\ k_{on}$, all of the models predict that increases of k_{branch} and k_{cap} by a factor of two or more affect the growth velocity by $<10\%$. The approximate invariance of the velocity in the simulations comes from two scaling properties of the network-growth process. The first is that if all of the rate parameters are increased by a factor α, the growth rate also increases by the same factor. This is clear because all steps in the simulation occur at the faster rate. The second scaling property is that if k_{on} is increased by a factor β, leaving k_{branch} and k_{cap} fixed, then the growth velocity increases by approximately a factor of β. This follows because the average orientation of the filaments impinging on the obstacle remains the same, but their growth rate is increased. Using these scaling laws sequentially, and choosing the scaling parameters so that $\alpha\beta = 1$, we find that the growth velocity is unaffected when k_{cap} and k_{branch} are scaled by the same factor. An experimental finding of a gross violation of this scaling property would point to the importance of other energy factors that are not scale-invariant, for example electrostatic energies.

It should also be possible to test the force-velocity and force-density relations shown in Fig. 10 in bead motility experiments. I can see two ways of doing this. First, one could freeze the bead in a laser trap with varying intensities. By measuring the position of the bead relative to the center of the trap, one can measure the force acting on it. Alternatively, the force can be varied by changing the bead's mobility. This can be done by changing its size. However, this should be done in such a way that the contact area of the actin network with the bead remains constant; otherwise, the effects of the varying contact area complicate the interpretation of the experiments. Achieving a fixed contact area could be accomplished by limiting the region on the bead coated by ActA to an area that is the same for all the beads. By evaluating the filament density as a function of the bead mobility and thus the force, one can establish the limits of the validity of models of the type presented here.

Future simulation work in this vein should aim to include the major effects missing here, in particular filament elasticity, correlation of branching orientation with filament twist, monomer-depletion effects, electrostatic interactions between filaments, and attachment to the obstacle. In addition, developing an analytic theory of the steady-state density and its force dependence would provide support for the generality of the results obtained here.

I am grateful to John Cooper for stimulating my interest in this project, and to Saveez Saffarian, Elliot Elson, and Jonathan Katz for informative conversations.

This research was supported by the National Institutes of Health Grant GM38542-12.

REFERENCES

Abraham, V. C., V. Krishnamurthi, D. L. Taylor, and F. Lanni. 1999. The actin-based nanomachine at the leading edge of migrating cells. *Biophys. J.* 77:1721–1732.

Bailly, M., F. Macaluso, M. Cammer, A. Chan, and J. E. Segall. 1999. Relationship between Arp2/3 complex and the barbed ends of actin filaments at the leading edge of carcinoma cells after epidermal growth factor stimulation. *J. Cell Biol.* 145:331–345.

Blanchoin, L., K. J. Amann, H. N. Higgs, J.-P. Marchand, D. A. Kaiser, and T. D. Pollard. 2000a. Direct observation of dendritic actin filament networks nucleated by Arp2/3 complex and WASp/SCAR proteins. *Nature.* 404:1007–1011.

Blanchoin, L., T. D. Pollard, and R. D. Mullins. 2000b. Interactions of ADF/cofilin, Arp2/3 complex, capping protein and profilin in remodeling of branched actin filament networks. *Curr. Biol.* 10:1273–1282.

Borisy, G. G., and T. M. Svitkina. 1999. Actin machinery: pushing the envelope. *Curr. Biol.* 12:104–112.

Carlier, M.-F., and D. Pantaloni. 1997. Control of actin dynamics in cell motility. *J. Mol. Biol.* 269:459–467.

Cameron, L. A., M. J. Footer, A. van Oudenaarden, and J. A. Theriot. 1999. Motility of ActA protein-coated microspheres driven by actin polymerization. *Proc. Natl. Acad. Sci.* 96:4908–4913.

Cameron, L. A., T. M. Svitkina, D. Vignjevic, J. A. Theriot, and G. G. Borisy. 2001. Dendritic organization of actin comet tails. *Curr. Biol.* 11:130–135.

Carlsson, A. E. 2000. The force-velocity relation for growing biopolymers. *Phys. Rev. E.* 62:7082–7091.

Dufort, P. A., and C. J. Lumsden. 1993. Cellular automation model of the actin cytoskeleton. *Cell Motil. Cytoskeleton.* 25:87–104.

Gittes, F., B. Mickey, J. Nettleton, and J. Howard. 1993. Flexural rigidity of microtubules and actin-filaments measured from thermal fluctuations in shape. *J. Cell Biol.* 120:923–924.

Gouin, E., H. Gantelet, I. Lasa, H. Ohayon, V. Villiers, P. Gounon, and P. J. Sansonetti. 1999. A comparative study of the actin-based mobilities of the pathogenic bacteria *Listeria monocytogenes*, *Shigella flexneri*, and *Rickettsia conorrii*. *J. Cell Sci.* 112:1697–1708.

Hartwig, J. H., G. M. Bokoch, C. L. Carpenter, P. A. Janmey, and L. A. Taylor. 1995. Thrombin receptor ligation and activated Rac uncap actin filament barbed ends through phosphoinositide synthesis and permeabilized human platelets. *Cell.* 82:643–653.

Higgs, H. N., and T. D. Pollard. 2000. Activation by Cdc42 and PIP2 of Wiskott-Aldrich syndrome protein (WASp) stimulates actin nucleation by Arp2/3 complex. *J. Cell Biol.* 150:1131–1320.

Huang, M., C. Yang, D. A. Schafer, J. A. Cooper, H. N. Higgs, and S. H. Zigmond. 1999. Cdc42-Induced Actin Filaments are Protected from Capping Protein. *Curr. Biol.* 9:979–982.

Isambert, H., P. Venier, A. C. Maggs, A. Fattoum, R. Kassab, D. Pantaloni, and M. F. Carlier. 1995. Flexibility of actin-filaments derived from thermal fluctuations: effect of bound nucleotide, phalloidin, and muscle regulatory proteins. *J. Biol. Chem.* 270:11437–11444.

Kuo, S. C., and J. L. McGrath. 2000. Steps and Fluctuations of *Listeria monocytogenes* during actin-based motility. *Nature.* 407:1026–1029.

Lanni, F., and B. R. Ware. 1984. Detection and characterization of actin monomers, oligomers, and filaments in solution by measurement of fluorescence photobleaching recovery. *Biophys. J.* 46:97–110.

Loisel, T. P., R. Boujemaa, D. Pantaloni, and M.-F. Carlier. 1999. Reconstitution of actin-based motility of *Listeria* and *Shigella* using pure proteins. *Nature.* 401:613–616.

McGrath, J. L., Y. Tardy, C. F. Dewey, J. J. Meister, and J. H. Hartwig. 1998. Simultaneous measurements of actin filament turnover, filament faction, and monomer diffusion in endothelial cells. *Biophys. J.* 75: 2070–2078.

Mogilner, A., and G. Oster. 1996. Cell motility driven by actin polymerization. *Biophys. J.* 71:3030–3045.

Mullins, R. D., J. A. Heuser, and T. D. Pollard. 1998. The interaction of Arp2/3 complex with actin: nucleation, high-affinity pointed end capping, and formation of branching networks of filaments. *Proc. Natl. Acad. Sci. U.S.A.* 95:6181–6186.

Olbris, D. J., and J. Herzfeld. 2000. Reconstitution of *Listeria* Motility: implications for the mechanism of force transduction. *Biochim. Biophys. Acta-Mol. Cell Res.* 1495:140–149.

Ott, A., M. Magnasco, A. Simon, and A. Libchaber. 1993. Measurement of the persistence length of polymerized actin using fluorescence microscopy. *Phys. Rev. E.* 48:R1642–R1645.

Pantaloni, D., R. Boujemaa, D. Didry, P. Gounon, and M.-F. Carlier. 2000. The Arp2/3 complex branches filament barbed ends: functional antogonism with capping proteins. *Nat. Cell Biol.* 2:385–391.

Peskin, C. S., G. M. Odell, and G. F. Oster. 1993. Cellular motions and thermal fluctuations: the Brownian ratchet. *Biophys. J.* 65:316–342.

Pollard, T. D. 1986. Rate constants for the reactions of ATP- and ADP-actin with the ends of actin filaments. *J. Cell Biol.* 103:2747–2754.

Pollard, T. D., L. Blanchoin, and R. D. Mullins. 2000. Molecular mechanisms controlling actin filament dynamics in nonmuscle cells. *Annu. Rev. Biophys. Biomol. Struct.* 29:545–576.

Riveline, D., C. H. Wiggins, R. E. Goldstein, and A. Ott. 1997. Elastohydrodynamic study of actin filaments using fluorescence microscopy. *Phys. Rev. E.* 56:1330–1334.

Schafer, D. A., P. B. Jennings, and J. A. Cooper. 1996. Dynamics of capping protein and actin assembly in vitro: uncapping barbed ends by polyphosphoinositides. *J. Cell Biol.* 135:169–179.

Sechi, A. S., J. Wehland, and J. V. Small. 1997. The isolated comet tail pseudopodium of *Listeria monocytogenes*: a tail of two actin filament populations, long and axial and short and random. *J. Cell Biol.* 137: 155–167.

Small, J. V. 1988. The actin cytoskeleton. *Electron Microsc. Rev.* 1:155–174.

Small, J. V., M. Herzog, and K. Anderson. 1995. Actin filament organization in the fish keratocyte lamellipodium. *J. Cell. Biol.* 139: 1275–1286.

Svitkina, T. M., A. B. Verkhovsky, K. M. McQuade, and G. G. Borisy. 1997. Analysis of the actin-myosin II system in fish epidermal keratocytes: mechanism of cell body translocation. *J. Cell Biol.* 139: 397–415.

Svitkina, T. M., and G. G. Borisy. 1999. Arp2/3 complex and actin depolymerizing factor/cofilin in dendritic organization and treadmilling of actin filament array in lamellipodia. *J. Cell Biol.* 145:1009–1026.

Tang, J. X., and P. A. Janmey. 1996. The polyelectrolyte nature of F-actin and the mechanism of actin bundle formation. *J. Biol. Chem.* 271: 8556–8563.

van Kirk, L. S., S. F. Hayes, and R. A. Heinzen. 2000. Ultrastructure of *Rickettsia rickettsii* actin tails and localization of cytoskeletal proteins. *Infect. Immun.* 68:4706–4713.

Weaver, A. M., A. V. Kariginox, A. W. Kinley, S. A. Weed, Y. Li, J. T. Parsons, and J. A. Cooper. 2001. Cortactin promotes and stabilizes Arp2/3-induced actin filament network formation. *Curr. Biol.* 11: 370–374.

Welch, M. D., J. Rosenblatt, J. Skoble, D. A. Portnoy, and T. J. Mitchison. 1998. Interaction of human Arp2/3 complex and the *Listeria monocytogenes* ActA protein in actin filament nucleation. *Science.* 281:105–108.

Wong, G. C. L., J. X. Tang, A. Lin, Y. Li, P. A. Janmey, and C. R. Safinya. 2000. Hierarchical self-assembly of F-actin and cationic lipid complexes: stacked three-layer tubule networks. *Science*. 288: 2035–2039.

Zigmond, S. H., M. Joyce, C. Yang, K. Brown, M. Huang, and M. Pring. 1998. Mechanism of Cdc42-induced actin polymerization in neutrophil extracts. *J. Cell Biol.* 142:1001–1012.